Chemical Science

EDGE ARTICLE

View Article Online
View Journal | View Issue



Cite this: *Chem. Sci.*, 2018, **9**, 1989

# A water-soluble supramolecular complex that mimics the heme/copper hetero-binuclear site of cytochrome *c* oxidase†‡

Hiroaki Kitagishi, *[a] Daiki Shimoji,[a] Takehiro Ohta,[b] Ryo Kamiya,[a] Yasuhiro Kudo,[a] Akira Onoda,[c] Takashi Hayashi,[c] Jean Weiss,[d] Jennifer A. Wytko[d] and Koji Kano[a]

Received 2nd November 2017
Accepted 12th January 2018

DOI: 10.1039/c7sc04732k

rsc.li/chemical-science

In mitochondria, cytochrome *c* oxidase (C*c*O) catalyses the reduction of oxygen ($O_2$) to water by using a heme/copper hetero-binuclear active site. Here we report a highly efficient supramolecular approach for the construction of a water-soluble biomimetic model for the active site of C*c*O. A tridentate copper(II) complex was fixed onto 5,10,15,20-tetrakis(4-sulfonatophenyl)porphinatoiron(III) ($Fe^{III}$TPPS) through supramolecular complexation between $Fe^{III}$TPPS and a per-*O*-methylated β-cyclodextrin dimer linked by a (2,2′:6′,2″-terpyridyl)copper(II) complex ($Cu^{II}$TerpyCD$_2$). The reduced $Fe^{II}$TPPS/$Cu^{I}$TerpyCD$_2$ complex reacted with $O_2$ in an aqueous solution at pH 7 and 25 °C to form a superoxo-type $Fe^{III}$–$O_2^-$/$Cu^{I}$ complex in a manner similar to C*c*O. The pH-dependent autoxidation of the $O_2$ complex suggests that water molecules gathered at the distal Cu site are possibly involved in the $Fe^{III}$–$O_2^-$/$Cu^{I}$ superoxo complex in an aqueous solution. Electrochemical analysis using a rotating disk electrode demonstrated the role of the FeTPPS/CuTerpyCD$_2$ hetero-binuclear structure in the catalytic $O_2$ reduction reaction.



## Introduction

Cytochrome *c* oxidase (C*c*O) is the terminal enzyme in the mitochondrial respiratory chain. C*c*O consumes most of the molecular oxygen ($O_2$) processed by living organisms by reducing it to water ($H_2O$).[1] The four-electron/four-proton reduction process ($O_2 + 4e^- + 4H^+ \rightarrow 2H_2O$) takes place at the heme $a_3$/$Cu_B$ hetero-binuclear active centre of C*c*O (Fig. 1a).[1–5] For the catalytic $O_2$ reduction reaction, the reaction mechanism schematically depicted in Fig. 1b has been proposed.[1–3] In the catalytic cycle, the fully reduced heme $a_3$/$Cu_B$ site ($Fe^{II}$/$Cu^{I}$, compound R) reacts with $O_2$ to form an oxymyoglobin-like superoxo complex of heme $a_3$ ($Fe^{III}$–$O_2^-$/$Cu^{I}$, compound A).[3,6] Compound A is rapidly (~0.5 ms) converted to an oxoferryl intermediate ($Fe^{IV}$=O/$Cu^{II}$–OH, compound P) *via* O–O bond cleavage assisted by H atom injection from a vicinal tyrosine residue.[3–6] Mechanistic investigations have suggested that one or more water molecules near the bound $O_2$ can facilitate the conversion of compound A to compound P.[7,8]

To understand the reaction mechanism, synthetic heme/copper models have been constructed using tetraarylporphinatoiron(II) ($PFe^{II}$) combined with $Cu^{I}$ complexes ($Cu^{I}L_n$, where L is a nitrogen donor ligand; *n* (coordination number) = 3 or 4).[4,5] However, upon oxygenation of the $PFe^{II}$/$Cu^{I}L_n$ model systems in anhydrous organic solvents, μ-peroxo-type bridged structures, *i.e.*, $PFe^{III}$–$O_2$–$Cu^{II}L_n$ complexes, tend to form instead of compound A-like superoxo species.[9–12] In native C*c*O, the μ-peroxo-type bridged structure has not been

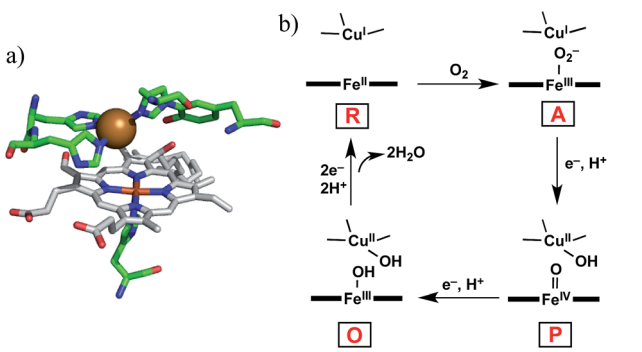


Fig. 1 (a) Heme $a_3$/$Cu_B$ hetero-binuclear active site of C*c*O (PDB ID: 1OCO) and (b) the simplified mechanism for the $O_2$ reduction reaction catalysed by C*c*O.

[a]*Department of Molecular Chemistry and Biochemistry, Faculty of Science and Engineering, Doshisha University, Kyotanabe, Kyoto 610-0321, Japan. E-mail: hkitagis@mail.doshisha.ac.jp*

[b]*Picobiology Institute, Graduate School of Life Science, University of Hyogo, RSC-UH LP Center, Hyogo 679-5148, Japan*

[c]*Department of Applied Chemistry, Graduate School of Engineering, Osaka University, 2-1 Yamadaoka, Suita 565-0871, Japan*

[d]*Institut de Chimie de Strasbourg, UMR 7177, CNRS, Université de Strasbourg, 4 Rue Blaise Pascal, 67000 Strasbourg, France*

† This paper is dedicated to (late) Professor Takashi Ogura.

‡ Electronic supplementary information (ESI) available. See DOI: 10.1039/c7sc04732k

experimentally identified, although it has been proposed as a transitional precursor of compound P.[3,12,13] The structural differences between the native and model systems (superoxo *vs.* μ-peroxo)[14] might be attributed to the influence of water.[7,8,13] A model study by Naruta and co-workers demonstrated that the μ-peroxo complex ($PFe^{III}$–$O_2$–$Cu^{II}L_3$) formed at −70 °C was converted to the superoxo complex ($PFe^{III}$–$O_2^-$/$Cu^{I}L_3$) at −30 °C by the action of water molecules.[15] In native C*c*O, highly ordered water molecules have been detected in the vicinity of heme $a_3$/$Cu_B$.[7,16] A quantum chemical calculation suggested that a water molecule in the vicinity of $Cu_B$ decreases the energy barrier of the transformation of compound A to compound P.[8] In this context, a water-soluble $PFe^{II}$/$Cu^{I}L_n$ model compound would be useful to investigate the role of water on the reactivity of the Fe/Cu hetero-binuclear complex with $O_2$. However, very few heme/copper mimics functioning under aqueous conditions have been prepared so far, except for the system constructed in the engineered heme pocket of myoglobin.[17,18]

In this study, we describe an aqueous synthetic PFe/$CuL_3$ hetero-binuclear model system built on a porphyrin/cyclodextrin supramolecular complex (Scheme 1). This system takes advantage of the very stable formation of a self-assembling 1 : 2 complex of 5,10,15,20-tetrakis(4-sulfonatophenyl)porphinatoiron (FeTPPS) with per-*O*-methylated β-cyclodextrins (CDs).[19] We have previously studied the porphyrin/cyclodextrin complexes as simple biomimetic models of heme proteins that function under aqueous conditions,[20–23] where the molecular cage of per-*O*-methylated β-CDs provided a microscopic hydrophobic environment for FeTPPS similar to the heme pocket of heme proteins.[24] Here, we have synthesised a per-*O*-methylated β-CD dimer linked by a $Cu^{II}$–terpyridine complex ($Cu^{II}TerpyCD_2$, Scheme 1) to replicate the distal tridentate $Cu_B$ site of C*c*O. The structural characterisation of the supramolecular FeTPPS/$CuTerpyCD_2$ complex and its reactivity towards $O_2$ are described.

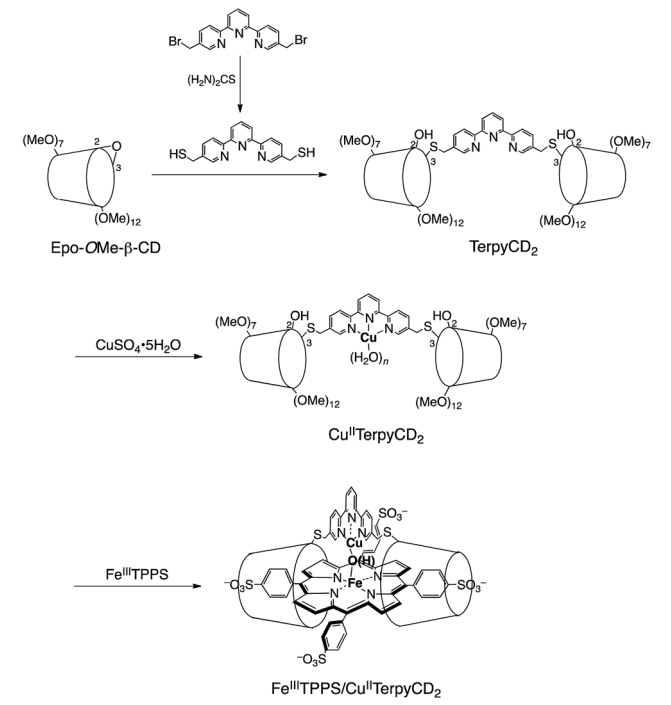


Scheme 1 Preparation of the supramolecular $Fe^{III}TPPS/Cu^{II}TerpyCD_2$ complex.

## Results and discussion

### Synthesis of a water-soluble $Fe^{III}/Cu^{II}$ hetero-binuclear complex

The synthetic route of a supramolecular $Fe^{III}TPPS/Cu^{II}TerpyCD_2$ complex is shown in Scheme 1 and experimental details are described in (ESI‡). Briefly, the terpyridyl ligand was inserted as a linker of the CD dimer ($TerpyCD_2$) by the reaction of 5,5″-bis(mercaptomethyl)-2,2′:6′,2″-terpyridine with 2,3-monoepoxy-per-*O*-methylated β-CD (Epo-*O*Me-β-CD).[20] The addition of $CuSO_4{\cdot}5H_2O$ to $TerpyCD_2$ in an aqueous solution generated two absorption bands at 336 and 350 nm (Fig. 2a), which corresponded to the ligand to metal charge transfer bands of the terpyridyl–$Cu^{II}$ 1 : 1 complex.[25] In the UV-vis titration, a biphasic spectral change was observed (Fig. 2a inset), indicating that the 1 : 2 complex of $Cu^{2+}$ with $TerpyCD_2$ ($\lambda_{max}$ = 333 nm) was first formed and then it was converted to the thermodynamically stable 1 : 1 complex upon further addition of $Cu^{2+}$. The spectral

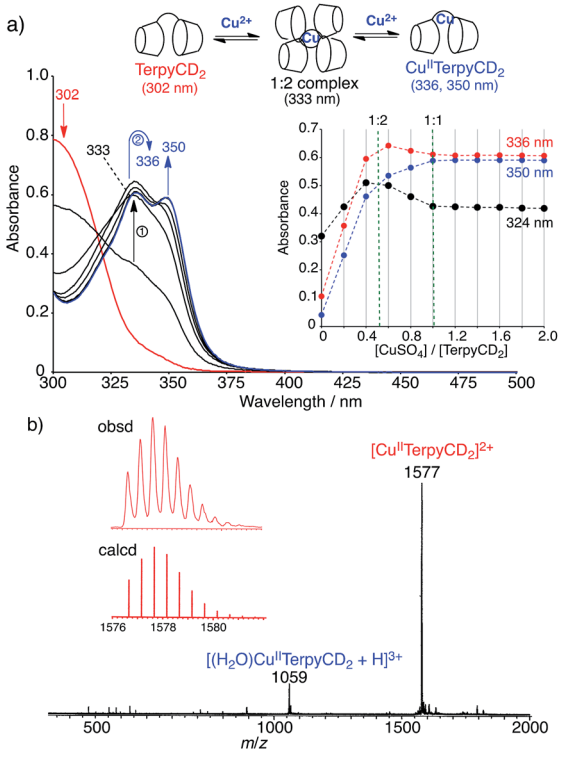


Fig. 2 Complexation of $TerpyCD_2$ with $Cu^{2+}$ in aqueous solution. (a) UV-vis spectral change of $TerpyCD_2$ (33 μM) upon stepwise addition of $CuSO_4$ in water at 25 °C. The inset shows changes in absorbances as a function of [$CuSO_4$]/[$TerpyCD_2$]. The biphasic titration curve indicates transient formation of the 1 : 2 complex before forming the thermodynamically stable 1 : 1 complex ($Cu^{II}TerpyCD_2$) during the titration. (b) Electrospray mass spectrum (positive mode) of the 1 : 1 mixture of $TerpyCD_2$ and $CuSO_4$ in $H_2O$. The inset shows the simulated isotope distribution patterns for the $[Cu^{II}TerpyCD_2]^{2+}$ complex.

changes were completed at one equivalent of $Cu^{2+}$. The complexation between $TerpyCD_2$ and $Cu^{2+}$ was also monitored by electrospray mass spectroscopy. In the 1 : 1 mixture of $CuSO_4$ and $TerpyCD_2$ in $H_2O$, the 1 : 1 complex ($Cu^{II}TerpyCD_2$) was observed at *m*/*z* 1577 and 1059 (Fig. 2b), which corresponds to $[Cu^{II}TerpyCD_2]^{2+}$ and $[(H_2O)Cu^{II}TerpyCD_2 + H]^{3+}$, respectively. The 1 : 2 complex was also detected as a small ion peak when the 1 : 2 mixture of $CuSO_4$ and $TerpyCD_2$ in $H_2O$ was analysed by electrospray mass spectroscopy (data not shown).

The $Cu^{II}TerpyCD_2$ complex was then titrated with $Fe^{III}TPPS$ (Fig. 3a). The Soret band of $Fe^{III}TPPS$ shifted from 408 nm to 418 nm, indicating that a μ-oxo-dimer of $Fe^{III}TPPS$ dissociated to the monomeric monohydroxo complex ($Fe^{III}(OH^-)TPPS$)[19] through interaction with $Cu^{II}TerpyCD_2$. The spectral changes were completed upon addition of one equivalent of $Cu^{II}TerpyCD_2$ to $Fe^{III}TPPS$, indicating a quantitative 1 : 1 complexation. The obtained complex was then analysed by electrospray mass spectroscopy. The two main ion peaks were detected at *m*/*z* 1385 and 2078 as tri- and di-anionic species, respectively (Fig. 3b). Considering total charges of the complexes, the peaks at *m*/*z* 1385 and 2078 were assigned to the μ-oxo and μ-hydroxo $Fe^{III}TPPS/Cu^{II}TerpyCD_2$ complexes, *i.e.*, $[PFe^{III}–O–Cu^{II}CD_2]^{3-}$ and $[PFe^{III}–(OH)–Cu^{II}CD_2]^{2-}$, respectively. The assignments were confirmed by isotope pattern simulations (Fig. 3b inset). Evidence of the μ-oxo ($Fe^{III}–O–Cu^{II}$) structure was also provided by its characteristic absorption bands at 453 and 567 nm, which appeared when the pH of the solution was increased (Fig. S3‡). The red-shifted Soret band at alkaline conditions indicates formation of the $PFe^{III}–O–Cu^{II}$ μ-oxo complex.[26–28] The pH titration revealed the acid–base equilibrium of $[PFe^{III}–O–Cu^{II}CD_2]^{3-}$ and $[PFe^{III}–(OH)–Cu^{II}CD_2]^{2-}$ with $pK_a = 8.8$. This $pK_a$ value is consistent with that previously predicted by Karlin and Blackburn ($pK_a = 8 \pm 2.5$).[28] The electron paramagnetic resonance (EPR) spectra showed significantly weak signals at $g = 6.09$ and 2.08 in the $Fe^{III}TPPS/Cu^{II}TerpyCD_2$ complex (Fig. S4‡) because of the antiferromagnetic coupling between the two metal ions as a result of their close proximity. The optimized molecular structure (Fig. 4) also illustrates the proximity of Fe and Cu ions in the $Fe^{III}TPPS/Cu^{II}TerpyCD_2$ complex; the Fe/Cu distances for the non-bridged and oxo-bridged forms are 5.23 and 3.52 Å, respectively. The distances are similar to those in native C*c*O, in which the oxidised heme $a_3/Cu_B$ distance were found in the range of 4.4–4.9 Å.[4]

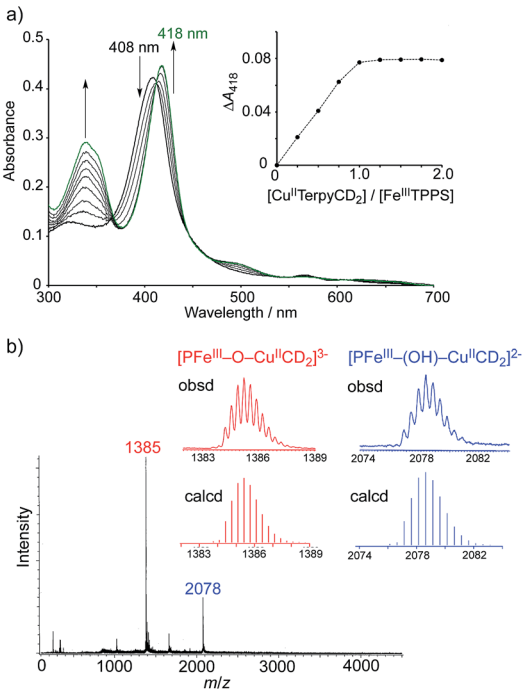


Fig. 3 Characterisation of the supramolecular $Fe^{III}TPPS/Cu^{II}TerpyCD_2$ complex. (a) UV-vis spectral changes of $Fe^{III}TPPS$ (3 μM) upon stepwise addition of $Cu^{II}TerpyCD_2$ in 0.05 M phosphate buffer at pH 7.0 and 25 °C. The inset shows the changes in absorbance at 418 nm as a function of the molar ratio ($[Cu^{II}TerpyCD_2]/[Fe^{III}TPPS]$). (b) Electrospray mass spectrum (negative mode) of the 1 : 1 mixture of $Fe^{III}TPPS$ and $Cu^{II}TerPyCD_2$ in $H_2O$. The inset shows the simulated isotope distribution patterns for the μ-oxo- and μ-hydroxo-bridged $Fe^{III}TPPS/Cu^{II}TerpyCD_2$ complexes.

## Characterisation of an $O_2$ adduct of the $Fe^{II}/Cu^{I}$ complex

The $Fe^{III}TPPS/Cu^{II}TerpyCD_2$ complex was reduced with excess sodium dithionite ($Na_2S_2O_4$) to obtain the fully reduced $[PFe^{II}/Cu^{I}CD_2]^{3-}$ complex in the deoxy state in an $O_2$-free solution ($\lambda_{max}$ at 430, 554, and 601 nm, Fig. 5, black line). The dissolved $O_2$ in the solution was completely consumed by excess dithionite, and the redox potential of dithionite is negative

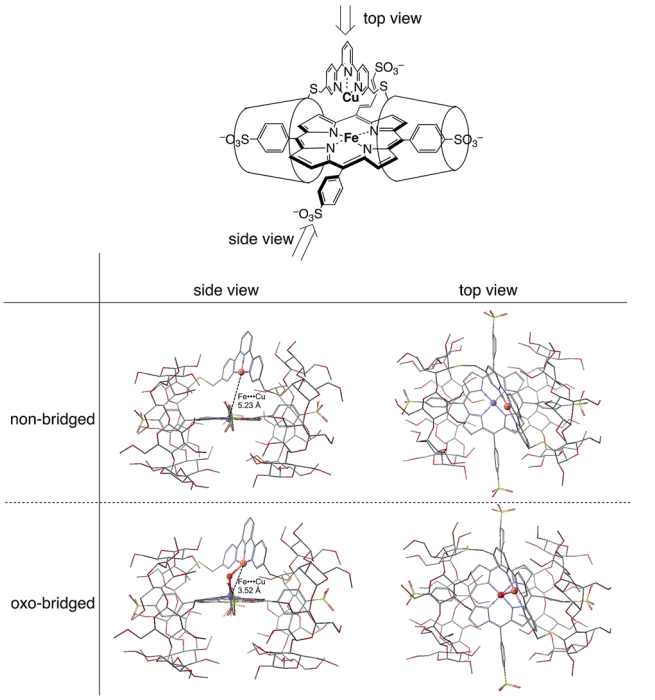


Fig. 4 Optimized molecular structures of the $FeTPPS/CuTerpyCD_2$ inclusion complexes in the Fe/Cu non-bridged and Fe/Cu oxo-bridged forms. The models are shown from both side and top views. Hydrogen atoms are omitted for clarity. Molecular mechanics calculations were carried out using CONFLEX/MM3 (extensive search) parameters in Scigress version 2.2.1 software program (Fujitsu).

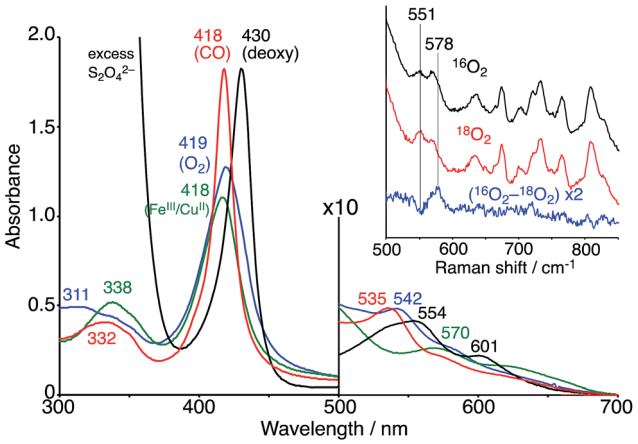


Fig. 5 UV-vis spectra of the $Fe^{III}$TPPS/$Cu^{II}$TerpyCD$_2$ (green) and its reduced $Fe^{II}$TPPS/$Cu^{I}$TerpyCD$_2$ complexes in the deoxy (black), oxy (blue) and CO (red) forms in 0.05 M phosphate buffer at pH 7.0 and 25 °C. The inset shows the resonance Raman spectra of the $Fe^{II}$TPPS/$Cu^{I}$TerpyCD$_2$ complexes obtained by excitation at 405 nm under $^{16}O_2$ atmosphere (black), $^{18}O_2$ atmosphere (red), and the difference $^{16}O_2$–$^{18}O_2$ (blue). Conditions: 0.05 M phosphate buffer at pH 7.0, 77 K (frozen solution).

Table 1 The Fe–O and O–O stretching frequencies ($\nu_{Fe-O}$/cm$^{-1}$, $\nu_{O-O}$/cm$^{-1}$) in the $O_2$ complexes of native C*c*O and synthetic PFe/CuL$_n$ compounds

| | $\nu_{Fe-O}$/cm$^{-1}$ $^{16}O_2$ ($^{18}O_2$) | $\nu_{O-O}$/cm$^{-1}$ $^{16}O_2$ ($^{18}O_2$) | Medium |
|---|---|---|---|
| **Superoxo group** | | | |
| C*c*O (beef heart)[a] | 572 (548) | — | $H_2O$, pH 7.4 |
| C*c*O (bovine heart)[b] | 571 (545) | — | $H_2O$, pH 7.2 |
| Fe/Cu[NMePr][c] | 570 (544) | — | $CH_2Cl_2$ |
| FeCuArOH[d] | 575 (549) | — | DMF |
| [($L^{N4\text{-}OH}$)Cu/Fe(TMPIm)][e] | 574 (548) | — | $CH_3CN$/THF |
| FeTPPS/CuTerpyCD$_2$[f] | 578 (551) | — | $H_2O$, pH 7.0 |
| **μ-Peroxo group** | | | |
| LS-4DCHIm[g] | 585, 591 (564) | 876, 863 (820) | MeTHF |
| [$L^{OH}$Fe/Cu][h] | — | 799 (752) | $CH_3CN$/toluene |
| [($L^{N4\text{-}OH}$)Cu/Fe(TMPIm)][e] | 611 (584) | 787, 803 (751) | $CH_3CN$/THF |

[a] Ref. 34. [b] Ref. 6. [c] Ref. 14. [d] Ref. 35. [e] Ref. 15. [f] This work. [g] Ref. 37. [h] Ref. 36.

enough to reduce both $Fe^{III}$ and $Cu^{II}$ to $Fe^{II}$ and $Cu^{I}$.[29,30] After the reduction, the solution was passed through a short gel-filtration column (Sephadex G-25) under aerobic conditions to remove excess $S_2O_4^{2-}$ and its oxidised products. The UV-vis spectrum of the resulting solution showed absorption maxima at 419 nm and 542 nm (Fig. 5, blue line); the Q-band was very different from that of the oxidised state ($Fe^{III}$TPPS/$Cu^{II}$TerpyCD$_2$, $\lambda_{max}$ (Q-band) = 570 nm, green line) and similar to that of the $O_2$ complex of the previously reported $Fe^{II}$TPPS/CD dimer system.[20] Introduction of CO gas into the solution caused further spectral changes with absorption maxima at 418 nm and 535 nm (Fig. 5, red line). The sharp Soret band is characteristic of the CO–$Fe^{II}$TPPS complex,[20] indicating that a ligand exchange from $O_2$ to CO occurs in this system.

The $O_2$ complex was further characterized by EPR and resonance Raman (rR) spectroscopic analyses. The EPR spectrum of the $O_2$ adduct of $Fe^{II}$TPPS/$Cu^{I}$TerpyCD$_2$ measured at 77 K was completely silent (Fig. S4‡), which was consistent with the spectra of other $O_2$ complexes of the PFe$^{II}$/Cu$^{I}$L$_n$ heterobinuclear systems.[31–33] The rR analysis at 77 K (frozen solution of the $O_2$ adduct) using 405 nm excitation revealed a characteristic band at 578 cm$^{-1}$, which shifted to 551 cm$^{-1}$ under an $^{18}O_2$ atmosphere (Fig. 5 inset). The isotope shift ($\Delta\nu$ = 27 cm$^{-1}$) corresponds to the expected value for the $\nu_{Fe-O}$ stretching mode.[15] The wavenumber is quite similar to those of the PFe$^{III}$–$O_2^-$/Cu$^{I}$L$_n$ superoxo complexes in the previously reported native[34] and synthetic model systems as listed in Table 1.[14,15,35] Furthermore, the O–O bond stretching mode ($\nu_{O-O}$) was not enhanced in this system. This is a relevant observation as the $\nu_{O-O}$ band is often observed in the range of 750–900 cm$^{-1}$ in the PFe$^{III}$–$O_2$–$Cu^{II}$L$_n$ μ-peroxo complexes, but not in the case of the Fe$^{III}$–$O_2^-$/Cu$^{I}$L$_n$ superoxo complexes (Table 1).[14,15,35–37] Based on the rR data, the configuration of the present $O_2$-adduct of $Fe^{II}$TPPS/$Cu^{I}$TerpyCD$_2$ is assigned as the superoxo-type PFe$^{III}$–$O_2^-$/Cu$^{I}$L$_3$ complex (Fig. 6), which is the same coordination mode as in compound A of native C*c*O.[3,14,38]

The superoxo PFe$^{III}$–$O_2^-$/Cu$^{I}$CD$_2$ complex was gradually converted to another state when the solution was allowed to stand at pH 7 and 25 °C under aerobic conditions (Fig. 7). The absorption spectra showed several isosbestic points and the final spectrum (shown as a green line in Fig. 7) was coincident to that of the oxidised $Fe^{III}$TPPS/$Cu^{II}$TerpyCD$_2$ complex (Fig. 5). EPR spectral changes also support oxidation of the superoxo PFe$^{III}$–$O_2^-$/Cu$^{I}$CD$_2$ species to the $Fe^{III}$TPPS/$Cu^{II}$TerpyCD$_2$ complex (Fig. S4‡). The first-order rate constants ($k_{obs}$) for the conversion were determined from the absorbance change at various pH conditions. Interestingly, the superoxo complex was more rapidly converted at lower pH (Fig. 7 inset). The linear pH/log $k_{obs}$ dependency at pH 7–10 (slope = −0.11) suggests that the conversion is partially accelerated by a proton-coupled process.[39] Collman *et al.* have reported that the rate of the $O_2$ reduction catalysed by their PFe/CuL$_n$ model complex is pH-dependent and increases at lower pH.[40] We have previously reported that the autoxidation rate of the $O_2$ complex in the PFe$^{II}$/CD dimer system without any distal functions is independent of pH in the neutral pH region (7–10), whereas it is accelerated at

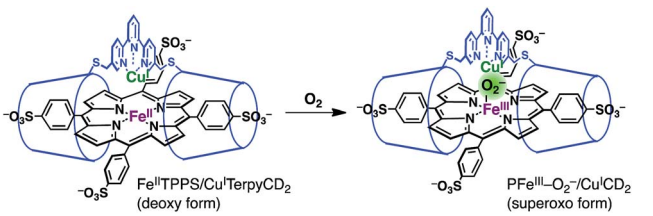


Fig. 6 Oxygenation of the $Fe^{II}$TPPS/$Cu^{I}$TerpyCD$_2$ complex to form a superoxo PFe$^{III}$–$O_2^-$/Cu$^{I}$CD$_2$ complex.

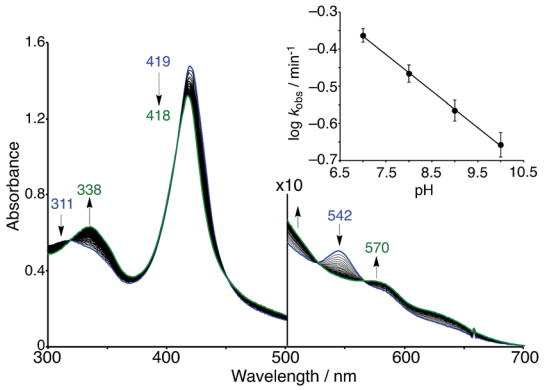


Fig. 7 Spontaneous conversion of the superoxo ($PFe^{III}$–$O_2^-$/$Cu^ICD_2$) complex in 0.05 M phosphate buffer at pH 7.0 and 25 °C. The spectrum was recorded at 15 s intervals. The inset shows the logarithmic first-order rate constants ($k_{obs}$) for the conversion as a function of the pH of the solution.

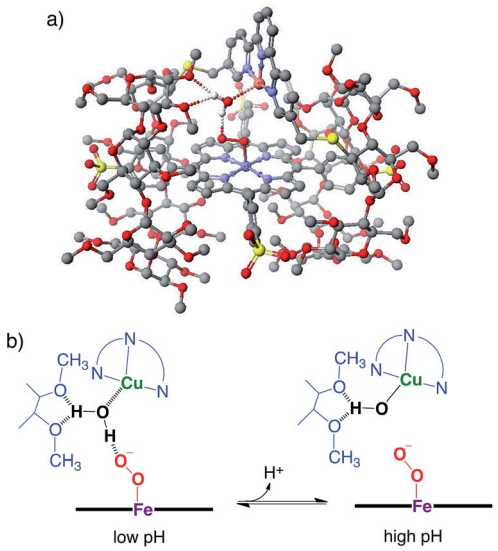


Fig. 8 The superoxo $PFe^{III}$–$O_2^-$/$Cu^ICD_2$ complex with a water molecule. (a) The molecular model constructed using CONFLEX/MM3 (extensive search) parameters in Scigress version 2.2.1 software program (Fujitsu). Hydrogen atoms, except for water, are omitted for clarity. (b) The possible acid–base equilibrium of the water, where the proton-donation to the superoxo $PFe^{III}$–$O_2^-$ moiety is likely to occur at low pH.

pH below 6 and above 10.[24] Therefore, the pH-rate dependency at the neutral pH region suggests that the water molecules gathered at the distal Cu site promote the conversion of the $PFe^{III}$–$O_2^-$/$Cu^ICD_2$ complex to the oxidised $PFe^{III}$–(OH)–$Cu^{II}CD_2$ complex.

The quantum chemical study on native C*c*O[8] proposes that a water molecule coordinating to the distal copper ion facilitates the conversion of compound A to compound P through the formation of the hydroperoxo $Fe^{III}$–OOH intermediate that has not been experimentally detected. Thus, the involvement of a water molecule in the present $PFe^{III}$–$O_2^-$/$Cu^ICD_2$ complex is likely to occur. In addition, molecular modelling suggests that a water molecule bound to the distal copper ion can induce protonation of the superoxo complex (Fig. 8a), where the methoxy groups of the CD dimer are suitable to provide two hydrogen bonding sites to the water. The pH-dependent decomposition of the superoxo complex, as shown in Fig. 7, might be explained by the acid–base equilibrium of the water molecule (Fig. 8b), where the proton-donation to the superoxo complex is likely to induce the O–O bond cleavage as proposed in C*c*O[8] and/or the proton-assisted autoxidation reaction similar to myoglobin.[41,42]

The $O_2$ binding in the present complex was practically irreversible; the $O_2$ complex of $Fe^{II}$TPPS/$Cu^I$TerpyCD$_2$ was never converted to its $Fe^{II}$/$Cu^I$ deoxy complex, even when the $O_2$ complex once formed was dissolved in a deoxygenated buffer (Fig. S5‡). In contrast, the deoxy complex was observed in the $Fe^{II}$TPPS/TerpyCD$_2$ complex without copper under the same experimental conditions.[43] This result indicates that the $O_2$ bound to $PFe^{II}$ is tightly held by the distal $Cu^IL_3$ complex, as previously demonstrated by the Fe/Cu superoxo complex.[14] The tight $O_2$ binding was also confirmed by observing ligand exchange with CO. The ligand exchange occurred slowly over ~30 min when the Fe/Cu superoxo complex was dissolved in a CO saturated buffer (Fig. S5‡), whereas it occurred instantaneously in the absence of distal Cu complex or in the absence of $O_2$ (Fig. S5‡). The ligand exchange of $O_2$ with CO also rapidly occurs in the previous $Fe^{II}$TPPS/CD dimer systems.[20,24] The significantly slow ligand exchange of $PFe^{II}$–$O_2^-$/$Cu^IL_3$ with CO caused by distal Cu complex might be related to the lower CO/$O_2$ affinity ratio of native C*c*O (0.1) in comparison to that of myoglobin (20–50) or haemoglobin (200–250).[44]

## Electrochemical analysis for the $O_2$ reduction

To evaluate the C*c*O-like function of this system, we monitored the electrocatalytic $O_2$ reduction reaction.[45–47] The cyclic voltammogram (CV) of the $Fe^{III}$TPPS/$Cu^{II}$TerpyCD$_2$ complex immobilized on a glassy carbon electrode showed a reversible redox couple at $E_{1/2} = -0.21$ V (*vs.* Ag/AgCl) in a deoxygenated buffer solution (under Ar, Fig. 9a, black line). The result is similar to those of the previously reported PFe/Cu$L_n$ heterobinuclear systems; the $Fe^{III}$/$Fe^{II}$ and $Cu^{II}$/$Cu^I$ redox waves appear at the same potentials.[31,46] In an air-saturated buffer, the CV of the $Fe^{III}$TPPS/$Cu^{II}$TerpyCD$_2$ complex showed a large catalytic current below −0.25 V because of $O_2$ reduction (Fig. 9a, blue line). A comparison of the CVs of the $Fe^{III}$TPPS/$Cu^{II}$TerpyCD$_2$ complex with those of the reference samples, *i.e.*, $Fe^{III}$TPPS and $Fe^{III}$TPPS/TerpyCD$_2$ (Fig. 9b), clearly indicates the effect of the Fe/Cu hetero-binuclear structure in the $O_2$ reduction; the $Fe^{III}$TPPS/$Cu^{II}$TerpyCD$_2$ complex showed a very large catalytic current starting from a lower onset potential ($\Delta E_{onset} = -40$ mV). The $O_2$ reduction process was then studied by linear sweep voltammetry (LSV) using a rotating disk electrode (RDE, Fig. 9c). The LSVs of the $Fe^{III}$TPPS/$Cu^{II}$TerpyCD$_2$ and $Fe^{III}$TPPS/TerpyCD$_2$ complexes showed diffusion limited catalytic $O_2$-reduction currents below −1.0 V *vs.* Ag/AgCl. In the case of FeTPPS without the CD dimer, the current was never saturated in LSV due to a slow reaction rate of the iron porphyrin with $O_2$

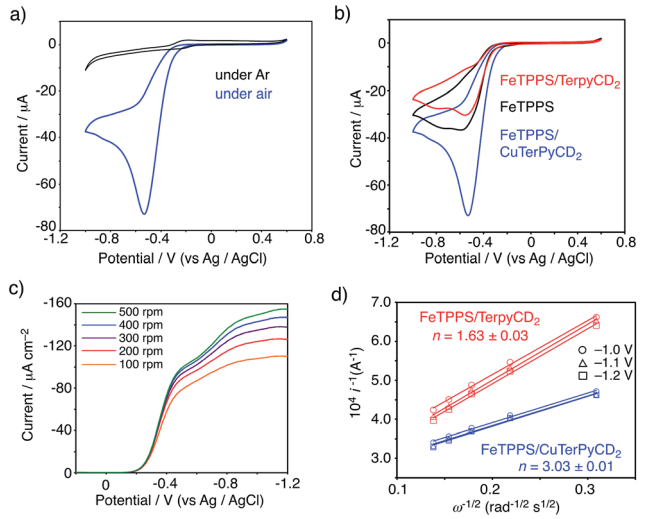


Fig. 9 (a, b) CV of the FeTPPS/CuTerpyCD$_2$ complex and its reference samples absorbed on the glassy carbon electrode with Nafion (5 wt% dispersion, 10 μL) in pH 7 phosphate buffer at a scan rate of 0.1 V s$^{-1}$ using Ag/AgCl and Pt wire as the reference counter electrodes, respectively. (c) LSV data for the FeTPPS/CuTerpyCD$_2$ complex (10 nmol) coated with Nafion (5 wt% dispersion, 10 μL) on a glassy carbon electrode in air saturated pH 7.0 phosphate buffer at a scan rate of 10 mV s$^{-1}$ at multiple rotations using Ag/AgCl and a Pt wire as the reference and counter electrodes, respectively. (d) Koutecky–Levich plots for the FeTPPS/CuTerpyCD$_2$ and FeTPPS/TerpyCD$_2$ complexes at the potentials of −1.0, −1.1 and −1.2 V to determine the average number of electrons ($n$) used for the O$_2$ reduction reaction.

on the disk electrode (Fig. S6‡). The saturated currents observed in the Fe$^{III}$TPPS/Cu$^{II}$TerpyCD$_2$ and Fe$^{III}$TPPS/TerpyCD$_2$ complexes at various rotation rates were analysed using the Koutecky–Levich equation to determine the average number of electrons ($n$) used in the O$_2$ reduction (Fig. 9d).[48] A significant increase in the $n$ value was observed for the Fe/Cu hetero-binuclear complex ($n$ = 3.03 ± 0.01) compared to the control sample without copper ($n$ = 1.63 ± 0.03).[49] Therefore, we conclude that the terpyridyl Cu complex associated with FeTPPS in our model system facilitates the catalytic O$_2$ reduction as an electron source, as proposed in the mechanism of native C*c*O[3] and as proven using the synthetic model systems.[5,45,48]

## Conclusions

In conclusion, we have synthesized a water-soluble biomimetic model complex for the heme $a_3$/Cu$_B$ hetero-binuclear active centre of C*c*O by utilizing a supramolecular complexation, and characterised its reactivity with O$_2$. To the best of our knowledge, this is the first example of a totally synthetic C*c*O model that works in a completely aqueous solution. In common with compound A of native C*c*O, we have identified the PFe$^{III}$–O$_2^-$/Cu$^I$CD$_2$ superoxo complex as the O$_2$ adduct in our model system in aqueous solution, whereas the PFe$^{III}$–O$_2$–Cu$^{II}$L$_n$ μ-peroxo complexes tend to form in the other synthetic model systems in anhydrous organic solvents. The pH-dependent conversion of the PFe$^{III}$–O$_2^-$/Cu$^I$CD$_2$ superoxo complex to its oxidised μ-hydroxo PFe$^{III}$–(OH)–Cu$^{II}$CD$_2$ complex suggested the involvement of water molecules in the formation of the superoxo complex in aqueous solution. We believe that our aqueous model system will help to clarify the long-standing arguments with regard to the native and synthetic model systems in C*c*O chemistry.

## Conflicts of interest

The authors declare no conflict of interest.

## Acknowledgements

We thank (late) Prof. Takashi Ogura (University of Hyogo) for the use of rR instruments and helpful discussion. This work was financially supported by MEXT/JSPS KAKENHI (Grant No. 15H02569, 16K13092, 17H02208), the MEXT-Supported Program for the Strategic Research Foundation at Private Universities (2015–2019), the Naito Foundation, Iketani Science and Technology Foundation, and Suntory Foundation for Life Sciences. JW and TH thank financial support from the bilateral France–Japan ANR-JST program TMOL"Molecular Technology" project "MECANO" AI\R.1 4.JTIC.OOO2.O 1.

## Notes and references

1 G. T. Babcock, *Proc. Natl. Acad. Sci. U. S. A.*, 1999, **96**, 12971–12973.
2 S. Ferguson-Miller and G. T. Babcock, *Chem. Rev.*, 1996, **96**, 2889–2907.
3 S. Yoshizawa and A. Shimada, *Chem. Rev.*, 2015, **115**, 1936–1989.
4 E. Kim, E. E. Chufán, K. Kamaraj and K. D. Karlin, *Chem. Rev.*, 2004, **104**, 1077–1133.
5 J. P. Collman, R. Boulatov, C. J. Sunderland and L. Fu, *Chem. Rev.*, 2004, **104**, 561–588.
6 T. Ogura, S. Hirota, D. A. Proshlyakov, K. Shinzawa-Itoh, S. Yoshikawa and T. Kitagawa, *J. Am. Chem. Soc.*, 1996, **118**, 5443–5449.
7 K. Muramoto, K. Ohta, K. Shinzawa-Itoh, K. Kanda, M. Taniguchi, H. Nabekura, E. Yamashita, T. Tsukihara and S. Yoshikawa, *Proc. Natl. Acad. Sci. U. S. A.*, 2010, **107**, 7740–7745.
8 M. R. A. Blomberg, P. E. M. Siegbahn, G. T. Babcock and M. Wilkström, *J. Am. Chem. Soc.*, 2000, **122**, 12848–12858.
9 E. Kim, J. Shearer, S. Lu, P. Moënne-Loccoz, M. E. Helton, S. Kaderli, A. D. Zuberbühler and K. D. Karlin, *J. Am. Chem. Soc.*, 2004, **126**, 12716–12717.
10 T. Chishiro, Y. Shimazaki, F. Tani, Y. Tachi, Y. Naruta, S. Karasawa, S. Hayami and Y. Maeda, *Angew. Chem., Int. Ed.*, 2003, **42**, 2788–2791.
11 E. E. Chufán, S. C. Puiu and K. D. Karlin, *Acc. Chem. Res.*, 2007, **40**, 563–572.
12 S. Hematian, I. Garcia-Bosch and K. D. Karlin, *Acc. Chem. Res.*, 2015, **48**, 2462–2474.
13 A. W. Schaefer, M. T. Kieber-Emmons, S. M. Adam, K. D. Karlin and E. I. Solomon, *J. Am. Chem. Soc.*, 2017, **139**, 7958–7973.

14 J. P. Collman, C. J. Sunderland, K. E. Berg, M. A. Vance and E. I. Solomon, *J. Am. Chem. Soc.*, 2003, **125**, 6648–6649.
15 J.-G. Liu, Y. Naruta and F. Tani, *Angew. Chem., Int. Ed.*, 2005, **44**, 1836–1840.
16 M. Ralle, M. L. Verkhovskaya, J. E. Morgan, M. I. Verkhovsky, M. Wilkström and N. J. Blackburn, *Biochemisty*, 1999, **38**, 7185–7194.
17 J. A. Sigman, B. C. Kwok and Y. Lu, *J. Am. Chem. Soc.*, 2000, **122**, 8192–8196.
18 A. Bhagi-Damodaran, M. A. Michael, Q. Zhu, J. Reed, B. A. Sandoval, E. N. Mirts, S. Chakraborty, P. Moënne-Loccoz, Y. Zhang and Y. Lu, *Nat. Chem.*, 2017, **9**, 257–263.
19 K. Kano, H. Kitagishi, S. Tamura and A. Yamada, *J. Am. Chem. Soc.*, 2004, **126**, 15202–15210.
20 K. Kano, H. Kitagishi, M. Kodera and S. Hirota, *Angew. Chem., Int. Ed.*, 2005, **44**, 435–438.
21 H. Kitagishi, M. Tamaki, T. Ueda, S. Hirota, T. Ohta, Y. Naruta and K. Kano, *J. Am. Chem. Soc.*, 2010, **132**, 16730–16732.
22 K. Watanabe, H. Kitagishi and K. Kano, *Angew. Chem., Int. Ed.*, 2013, **52**, 6894–6897.
23 H. Kitagishi, S. Kurosawa and K. Kano, *Chem.–Asian J.*, 2016, **11**, 3213–3219.
24 K. Kano, H. Kitagishi, C. Dagallier, M. Kodera, T. Matsuo, T. Hayashi, Y. Hisaeda and S. Hirota, *Inorg. Chem.*, 2006, **45**, 4448–4460.
25 V. M. Manikandamathavan, V. Rajapandian, A. J. Freddy, T. Weyhermüller, V. Subramanian and B. U. Nair, *Eur. J. Med. Chem.*, 2012, **57**, 449–458.
26 M.-A. Kopf, Y.-M. Neuhold, A. D. Zuberbühler and K. D. Karlin, *Inorg. Chem.*, 1999, **38**, 3093–3102.
27 E. Kim, M. E. Helton, I. M. Wasser, K. D. Karlin, S. Lu, H.-w. Huang, P. Moënne-Loccoz, C. D. Incarvito, A. L. Rheingold, M. Honecker, S. Kaderli and A. D. Züberbuhler, *Proc. Natl. Acad. Sci. U. S. A.*, 2003, **100**, 3623–3628.
28 S. Fox, A. Nanthakumar, M. Wilkström, K. D. Karlin and N. J. Blackburn, *J. Am. Chem. Soc.*, 1996, **118**, 24–34.
29 S. G. Mayhew, *Eur. J. Biochem.*, 1978, **85**, 535–547.
30 B. Liu, Y. Chen, T. Doukov, S. M. Soltis, C. D. Stout and J. A. Fee, *Biochemistry*, 2009, **48**, 820–826.
31 Z. Halime, H. Kotani, Y. Li, S. Fukuzumi and K. D. Karlin, *Proc. Natl. Acad. Sci. U. S. A.*, 2011, **108**, 13990–13994.
32 P. Vorburger, M. Lo, S. Choua, M. Bernard, F. Melin, N. Oueslati, C. Boudon, M. Elhabiri, J. A. Wytko, P. Hellwig and J. Weiss, *Inorg. Chim. Acta*, 2017, **468**, 232–238.
33 C. Kahlfuss, J. A. Wytko and J. Weiss, *ChemPlusChem*, 2017, **4**, 584–594.
34 C. Varotsis, W. H. Woodruff and G. T. Babcock, *J. Biol. Chem.*, 1990, **265**, 11131–11136.
35 J. P. Collman, R. A. Decréau, Y. Yan, J. Yoon and E. I. Solomon, *J. Am. Chem. Soc.*, 2007, **129**, 5794–5795.
36 J.-G. Liu, Y. Naruta, F. Tani, T. Chishiro and Y. Tachi, *Chem. Commun.*, 2004, 120–121.
37 S. M. Adam, I. Garcia-Bosch, A. W. Schaefer, S. K. Sharma, M. A. Siegler, E. I. Solomon and K. D. Karlin, *J. Am. Chem. Soc.*, 2017, **139**, 472–481.
38 The $\nu_{Fe-O}$ stretching frequency of 578 $cm^{-1}$ is higher than the reported values for the penta-coordinated $PFe^{III}–O_2^-$ complexes, indicating that the Lewis acidity of the distal Cu complex significantly alters the Fe–O bonding. For the $\nu_{Fe-O}$ data of $PFe^{III}–O_2^-$ complexes, see: K. M. Vogel, P. M. Kozlowski, M. Z. Zgierski and T. G. Spiro, *J. Am. Chem. Soc.*, 1999, **121**, 9915–9921.
39 If this conversion would have been completely conjugated with the proton transfer, the slope of the pH/log $k_{obs}$ plot would be −1.0.
40 J. P. Collman, S. Ghosh, A. Dey, R. A. Decréau and Y. Yang, *J. Am. Chem. Soc.*, 2009, **131**, 5034–5035.
41 K. Shikama, *Chem. Rev.*, 1998, **98**, 1357–1373.
42 In the present system, any intermediate species ascribed to ferryloxo ($Fe^{IV}$=O) complex could not be observed during conversion from the superoxo to the oxidised complexes in aqueous solution at room temperature.
43 The $O_2$ complex was also formed in the $Fe^{II}$TPPS/TerpyCD$_2$ complex without copper. The UV-vis spectrum of this complex ($\lambda_{max}$ = 419 and 542 nm) was found to be consistent with that of the $PFe^{III}–O_2^-/Cu^{I}CD_2$ superoxo complex, which further supports the absence of a direct interaction between the distal $Cu^{I}$ and the bound $O_2$ in the $PFe^{III}–O_2^-/Cu^{I}CD_2$ complex.
44 R. Motterlini and R. Foresti, *Am. J. Physiol.: Cell Physiol.*, 2017, **312**, C302–C313.
45 J. P. Collman, N. K. Devaraj, R. A. Decréau, Y. Yang, Y.-L. Yan, W. Ebina, T. A. Eberspacher and C. E. D. Chidsey, *Science*, 2007, **315**, 1565–1568.
46 R. Boulatov, J. P. Collman, I. M. Shiryaeva and C. J. Sunderland, *J. Am. Chem. Soc.*, 2002, **124**, 11923–11935.
47 F. Melin, A. Trivella, M. Lo, C. Ruzié, I. Hijazi, N. Oueslati, J. A. Wytko, B. Boitrel, C. Boudon, P. Hellwig and J. Weiss, *J. Inorg. Biochem.*, 2012, **108**, 196–202.
48 S. Chatterjee, K. Sengupta, S. Hematian, K. D. Karlin and A. Dey, *J. Am. Chem. Soc.*, 2015, **137**, 12897–12905.
49 The selectivity of the electrocatalytic $O_2$ reduction by the FeTPPS/CuTerpyCD$_2$ and its copper free complexes could not be determined using a rotating ring disk electrode system because of very low currents detected at the ring electrode.